Seismic Behavior of Cast-in-Place and Precast Recycled Aggregate Concrete Frames: A Comparative Study

Jianzhuang Xiao, Dr.; **Tao Ding,** Civil Eng.; **Changqing Wang,** Dr.; Tongji University, Shanghai, China.
Contact: jzx@tongji.edu.cn
DOI: 10.2749/101686615X14210663188853

Abstract

Shaking table tests were carried out on two recycled aggregate concrete (RAC) frames, one of which was cast-in-place (CIP) and the other was precast. The dimensions and reinforcements of the two structures were designed similarly for the purpose of comparing seismic performance. The comparative analysis of the structural behavior indicated that both the models performed favorably with respect to their capacity for seismic resistance and presented similar dynamic response tendencies in the elastic and early nonlinear stage. In the later elasto-plastic stage, for the precast RAC frame, the deformation was relatively larger, the overall seismic capacity was lower and the stiffness degradation was faster compared to the CIP frame. A further analysis of the frame joints of the two frames was undertaken and it demonstrated that serious damage to the post-cast joints in the precast frame was the main reason for the inferior structural seismic behavior during earthquakes of high-level intensity.

Keywords: recycled aggregate concrete (RAC); cast-in-place (CIP); precast; seismic behavior.

Introduction

The rapid development of urbanization and the construction industry has witnessed an increase in the generation of construction and demolition waste. From the viewpoints of environmental preservation and effective utilization of resources, adopting recycled aggregate concrete (RAC) is a necessary and productive solution so as to conserve natural resources and reduce demolition waste.[1,2]

As a result, researchers have engaged in systematic investigations of the physical and mechanical properties of RAC. Achievements summarized in Refs. [3–8] have all shown that the mechanical properties of RAC may be generally lower than those of natural aggregate concrete (NAC). The replacement percentage of recycled coarse aggregates (RCAs) has a considerable influence on the stress–strain relationship of RAC under uniaxial compression and tensile loading. Furthermore, in order to apply RAC as a kind of structural material, a series of experimental studies on the seismic behavior of RAC structural components were also carried out by researchers worldwide. Experimental studies on RAC beams revealed that the shear capacity of reinforced RAC beams is comparable, or even superior, to that of beams made entirely with NAC, provided the mix proportion is designed appropriately.[9,10] Semi-precast columns with RAC investigated in Ref. [11] showed that RAC semi-precast columns have a good seismic behavior, similar to that of NAC columns. Behavior studies in Refs. [12, 13] found that cast-in-place (CIP) joints prepared with both 100 and 30% RCA replacements show an adequate cyclic behavior if the joints are suitably designed. Particularly, four 1:2 scaled plan frame specimens made of RAC under low-frequency cyclic lateral load were studied in Ref. [14]. Furthermore, shaking table tests were conducted to investigate the seismic performance of RAC frame–shear wall structures.[15] According to these studies, the general seismic performance of RAC structures declines with an increase in RCA replacement percentage. However, it has also been found from these tests that the RAC frame failure mechanism can be characterized in a manner of "strongest joints, stronger columns and weaker beams." The energy dissipation and stiffness degradation of RAC structures is comparable to that of conventional concrete structures; that is, RAC structures with a proper mix design are still good enough to resist earthquake shocks, in general. The positive results of these pioneering studies demonstrate the favorable structural performance of RAC and also provide the basic technical support for the safe application of RAC in structures of civil engineering.

Nowadays, contractors and researchers are suggesting that RAC components should be manufactured in factories.[16] Although the construction quality control is more difficult for RAC than NAC in the construction field, the prefabricated construction technology can ensure the construction quality of the RAC components and avoid the disadvantages of RAC preparation. Structural systems employing precast concrete elements made of RAC might, to some extent, promote the popularization of RAC and conform to the trend of industrialization.

However, most investigations on precast structures were focused on structures made with NAC. Studies conducted in Refs. [17–19] focused on the connections in precast frame structures. These authors proposed different kinds of available joints in prefabricated systems and provided several suggestions to improve their seismic performance. Furthermore, in the 1990s, a large-scale five-story precast concrete building, which was tested under simulated seismic loading[20] in the USA based on the precast seismic structural systems research program (PRESSS), showed that the structural behavior of this structure was satisfactory, with no significant capacity loss. Recently, a shaking table test was carried out at INCERC-Jassy in Romania, focusing on a 1:4 scaled five-story precast concrete structure. The results showed that the interstory drifts during the tests satisfied the requirements of the Romanian Seismic Design.[21] Applying RAC into precast products has already attracted the attention of experts and contractors, and some tentative investigations undertaken show similar mechanical properties when

Peer-reviewed by international experts and accepted for publication by SEI Editorial Board

Paper received: December 25, 2014
Paper accepted: March 30, 2015

using RAC in precast products such as concrete paving blocks and concrete pavement flags.[22,23] However, although the previous investigations demonstrated that precast concrete structures or products are available for application in structural engineering, there were no comparative tests focusing on a CIP structure to provide convincing conclusions. In particular, the difference between an RAC precast frame structure and a CIP structure with regard to seismic response has not been studied systematically to provide a clear understanding.

In this study, for the purpose of finding out the difference between the structural behaviors of two RAC frame structures, two shaking table tests on CIP and precast RAC frame models were designed, to provide a comprehensive contrast analysis of the seismic performance. A further analysis, particularly of the seismic behavior of the frame joints, was examined, in order to provide an intensive explanation for the discrepancy in the seismic performance of the two frames.

Description of Two Shaking Table Tests

Materials

For the purpose of drawing an intensive and credible seismic comparison between CIP and precast RAC frame structures, the same construction materials were used in the two models. For cement, a 28-day nominal compressive strength grade of 42.5 MPa was used in the RAC mixing. The applied coarse aggregates used in the concrete were RCAs with a particle diameter of between 5 and 10 mm. The recycled concrete mixture of nominal strength grade C30 was proportioned with the RCA replacement percentage equal to 100% in both the shaking table tests. The mix proportions of CIP RAC was water : cement : sand : RCAs = 1 : 1.887 : 2.301 : 3.312, while for the precast RAC, it was 1 : 1.859 : 3.202 : 4.554. The mechanical properties of the RCAs and RAC used in the tests were almost identical, which can be inferred from *Table 1*. More details about the material properties of RCAs and RAC can be found in Ref. [24]. For example, the average compressive strength of RAC was 38 MPa for the CIP model, and 38.2 MPa for the precast model; the apparent density of the RCAs used was 2520 kg/m^3 for the CIP model, and 2480 kg/m^3 for the precast model. Galvanized steel wires of 8# (diameter of 3.94 mm) and 10# (diameter of 3.32 mm) were adopted for the longitudinal reinforcements and 14# (diameter of 2.32 mm) for the transversal reinforcement in both the tested models.

Model frame	RCAs		RAC
	Apparent density (kg/m^3)	Water absorption (%)	Compressive strength (28 days) (MPa)
CIP	2520	11.55	38.0
Precast	2480	8.21	38.2

Table 1: Mechanical properties of the RCAs and RAC used

Design and Construction Details

The two models were designed by scaling down the geometry from one prototype structure and the dimension scaling parameter was taken as 1 : 4. The main similarity relations between the prototype and the models were derived from Buckingham π theorem[25]; more details are listed in *Table 2*.

Both the models were two-bay, two-span, and six-story frame structures regular in plane and elevation: they were 2175 × 2550 mm in plane, with a story height of 750 mm and a slab thickness of 30 mm. The details of the general geometry, the element sections, and the corresponding reinforcements of the beams and columns are shown in *Fig. 1a–c* for both *X* and *Y* directions. The reinforcing steel in the beam–column joints for the CIP model and the precast model, respectively, are shown in *Fig. 1d*. The designing frame satisfied the ACI 318-05[26] seismic design provisions. It is worth mentioning that, unlike the CIP frame, the beams of the precast RAC frame were designed as semi-precast beams and the top reinforcements of the beams were assembled on the post-cast construction area. In addition, a welding connection was adopted to link the longitudinal rebars of columns in the joint and the concrete of the joints or slabs was post-cast for the precast frame. *Figure 2a and b* shows the two models fixed on the shaking table, respectively.

Test Procedure

The test program of the two shaking table tests consisted of seven phases, that is, tests for peak ground acceleration (PGA) of 0.066 *g* (frequently occurring earthquakes of intensity 7), 0.130 *g* (frequently occurring earthquakes of intensity 8), 0.185 *g* (occasionally occurring earthquakes of intensity 7), 0.370 *g* (occasionally occurring earthquakes of intensity 8), 0.415 *g* (rarely occurring earthquakes of intensity 7), 0.550 *g* (rarely occurring earthquakes of intensity 8), and 0.750 *g* (maximum considered events) in *X* direction (*X* and *Y* directions are shown in *Fig. 1a*). According to Appendices G and I of the Seismology Committee[27] and the revisions proposed for the Appendix in the SEAOC Performance-Based Seismic Engineering Ad Hoc Subcommittee,[28] these seismic actions were identified as of four earthquake intensity levels EQ-1 (0.066 *g*-intensity 7; 0.130 *g*-intensity 8), EQ-2 (0.185 *g*-intensity 7; 0.370 *g*-intensity 8), EQ-3 (0.415 *g*-intensity 7; 0.550 *g*-intensity 8), and EQ-4 (0.750 *g*-intensity 8). These four levels of earthquakes were characterized as frequent, occasional, rare, and maximum considered events, having a mean return period of 25, 72, 250–800, and 800–2500 years, respectively. These test phases were set to evaluate the different seismic responses of the two structures including overall capacity and dynamic response.

As shown in *Fig. 3*, three earthquake waves, namely Wenchuan seismic wave (WCW, 2008, N-S), El Centro wave (ELW, 1940, N-S), and Shanghai artificial wave (SHW), were selected as the input seismic waves. WCW, ELW, and SHW were input in sequence during the test process. Accelerometers and displacement Linear Variable Differential Transducers (LVDTs) were installed in each floor of the two models to measure and compare the acceleration and displacement response during the shaking table tests. The installation locations of these sensors are shown in *Fig. 2c*.

Parameter	Length	Acceleration	Elasticity modulus	Time	Damping	Density
Model/prototype	0.250	1.848	1.000	0.368	0.092	2.164

Table 2: Similitude scale parameters of the two models

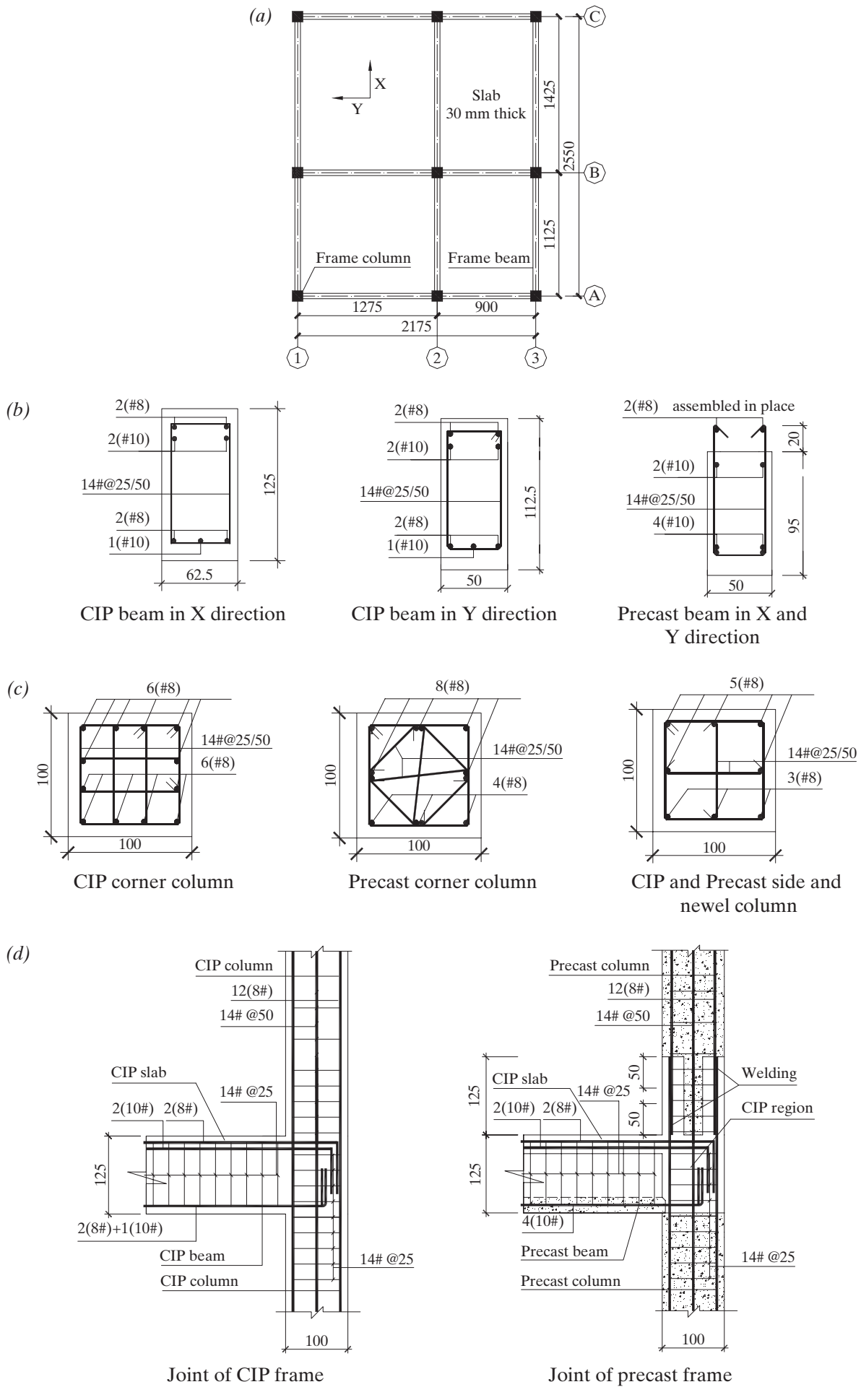

Fig. 1: Configuration and reinforcements for two RAC frame models. (a) Plan layout; (b) reinforcements for the frame beams; (c) reinforcements for the frame columns; (d) reinforcements for the frame joints (Unit: mm)

Seismic Response Comparison

Failure Patterns

During the first half of the shaking table tests, there were no obvious cracks appearing on the two models. However, at the end of the simulated earthquake tests, the major damages to both models eventually occurred, and propagated at the first and second stories with plastic hinges forming at the end of some beams. The width of flexural cracks increased with the models being subjected to an increasing intensity of earthquakes. The third floor was slightly damaged while no visible cracks were observed on the fourth to the sixth floors in both the models. Compared to the CIP frame, during the later stages of the tests, the precast frame exhibited relatively serious damages, with more horizontal and diagonal cracks spreading at the post-cast joints on the first and second floors. On the whole, during the shaking table tests it was observed that the first plastic hinge occurred at the first story beam end, and then at the second story beam end, as expected, for both the frames. In general, some slightly curving cracks emerged at the ends of some frame beams between the first and second stories during the test phases, with PGAs ranging from 0.185 to 0.550 *g*. Then several new fine cracks emerged at the top of the second story column. However, it was suggested on the basis of the test observation that the precast frame suffered more serious damage under the shear action of the earthquake. The crack development situation of typical beams and joints of the two RAC frame structures are shown vividly in *Fig. 4*.

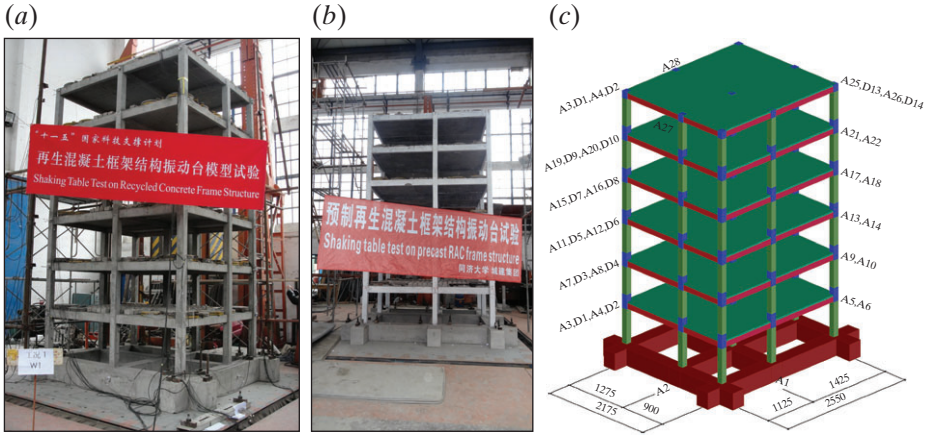

Fig. 2: Two RAC frame models on the shaking table and the installation of sensors. (a) CIP RAC frame in 2011; (b) precast RAC frame in 2013 and (c) installation of sensors

Dynamic Response

The dynamic characteristics such as frequency and damping ratio of a frame structure, which are related to the energy dissipation and absorption capacity, are crucial parameters

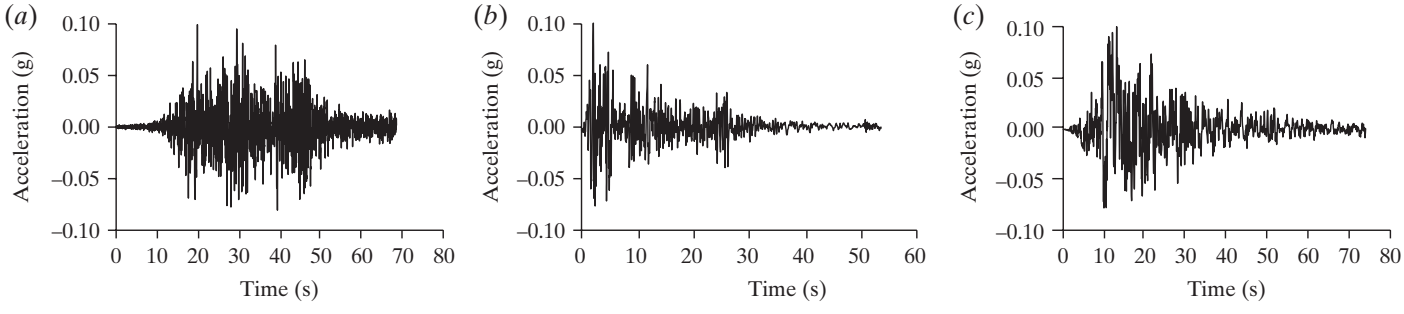

Fig. 3: Time history of the input seismic waves. (a) WCW; (b) ELW and (c) SHW

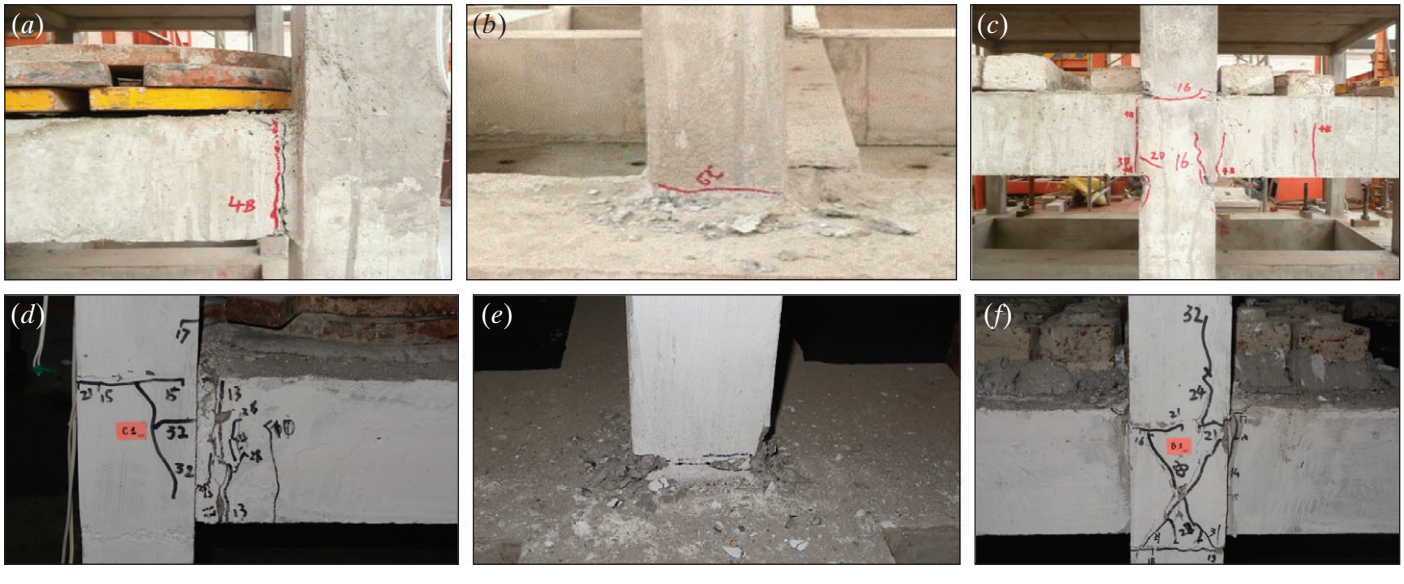

Fig. 4: Typical crack modes of the two RAC frames. (a) Cracks on the side part of CIP frame (first floor); (b) cracks on the column base of CIP frame (base); (c) cracks on the inner joint of CIP frame (first floor); (d) cracks on the beam end of precast frame (first floor); (e) cracks on the column base of precast frame (base) and (f) cracks on the inner joint of precast frame (first floor)

for earthquake-resistant design. Based on the shaking table tests, the natural vibration frequency of the structure was obtained through white noise scanning and transfer function curve dealing. Moreover, the well-known half-power bandwidth method was used to calculate the equivalent viscous damping ratios for the two frames. *Figure 5* demonstrates the variation of first order natural frequency and damping ratio of the two models in *X* direction. It can be inferred that in the first half of the tests, before 0.415 *g* of PGA (rarely occurring earthquakes of intensity 7), the frequency of the two models decreased progressively at almost the same rate in the elastic and early elasto-plastic stages; the damping ratio of the CIP model was slightly less than that of the precast frame, revealing that the structural damage caused by earthquake action was a bit smaller. In general, because of the slight damage that occurred to the two frames subjected to small ground motion excitations, the difference in seismic response was not so obvious for the two models during this stage. During the test case with PGA ranging from 0.550 to 0.750 *g* (rarely occurring earthquakes of intensity 8 to maximum considered events), that is, at the end of the tests, the frequency of the precast frame was slightly less than that of the CIP model, because of a relatively fast decreasing tendency, while the damping ratio of the precast model also increased somewhat more rapidly during this stage.

Based on the observation of failure patterns during the tests, this phenomenon was assumed to be caused by the more severely damaged post-cast joints of the precast model in the nonlinear stage, compared to the CIP model.

Roof Displacement and Interstory Drift

Figure 6 shows the maximum roof displacement and maximum interstory drift response of the two models when WCW, ELW, and SHW were input during different intensities of earthquakes. The diagram reveals that the lateral deformation curves of the two model structures were roughly the same when the same levels of seismic waves were input during the tests, including an average of the WCW, ELW, and SHW input.

During the test cases from 0.066 *g* (frequently occurring earthquakes of intensity 7) to 0.370 *g* (occasionally occurring earthquakes of intensity 8), with the increase in earthquake intensity, the roof displacement and interstory drift of the two models increased proportionally for each test phase. The maximum roof displacement and maximum interstory drift of the precast and CIP models were very close to each other, which meant that the seismic behavior of the two models was similar during these stages. However, in the later shaking table tests, the maximum roof displacement and maximum interstory drift of the precast frame structures were larger than those of the CIP structure, as clearly illustrated in *Fig. 6*.

It was found that during the whole test process, the maximum interstory drift commonly appeared at the first or the second floor among the first–sixth floors for both the models. In addition, the increasing amplitude for the maximum interstory drift of the first and second floors was greater than that of the third to the sixth floors. It was suggested that the damage level of the precast structure was more serious in the later test stages and the interstory stiffness degradation of the first and second floors was a bit faster.

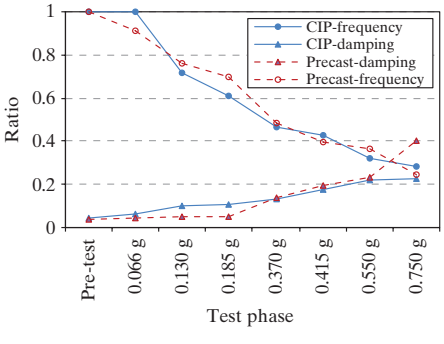

Fig. 5: Variation of frequency and damping ratio in X direction

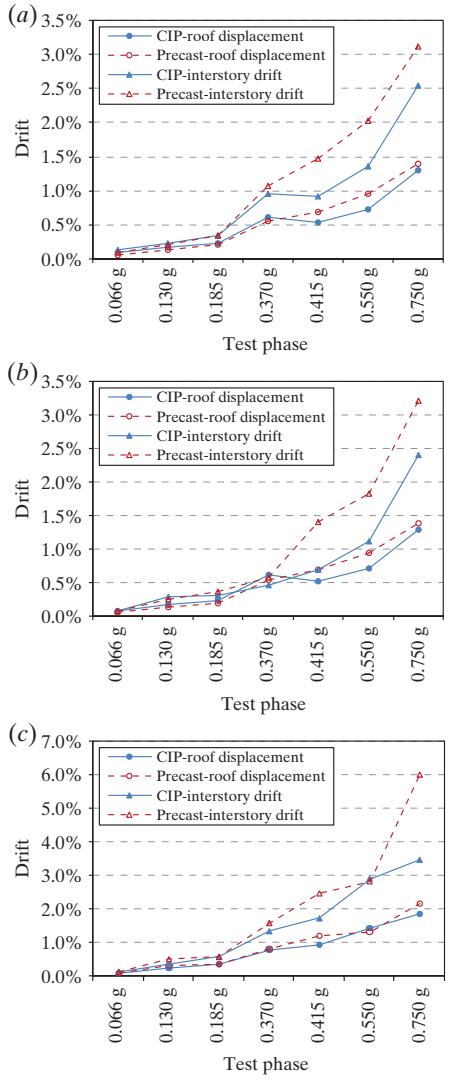

Fig. 6: Maximum roof displacement and maximum interstory drift. (a) Under WCW; (b) under ELW and (c) under SHW

Stiffness Degradation

Based on the initial structural stiffness, the stiffness degradation of the two models over the whole of the test phase was compared, as shown in *Fig. 7*. The stiffness of the frame decreases continuously under the seismic action, which can be described as the secant stiffness variation using base shear force and roof displacement.

$$K_i = \frac{|+F_i|+|-F_i|}{|+X_i|+|-X_i|} \quad (1)$$

where K_i is the secant stiffness of the i^{th} test case; F_i is the maximum shear force of the i^{th} test case; and X_i is the roof displacement corresponding to F_i in the i^{th} test case.

Figure 7 demonstrates the tendency of lateral stiffness degradation of the two models. During the early stages of the test phases, for example, with the PGA of 0.130 *g* (frequently occurring earthquakes of intensity 8), the stiffness of the precast model was even a little larger than that of the CIP model, which showed that the precast frame had a comparable seismic performance, whereas, after the test case of 0.370 *g* (occasionally occurring earthquakes of intensity 8), when the two models moved into the nonlinear stage, the stiffness of the precast frame reduced somewhat faster than that of the CIP structure, which was consistent with the previous comparative analysis of the displacement and dynamic response.

Envelop Curves

In *Fig. 8*, the envelop curves of the two models are depicted according to the

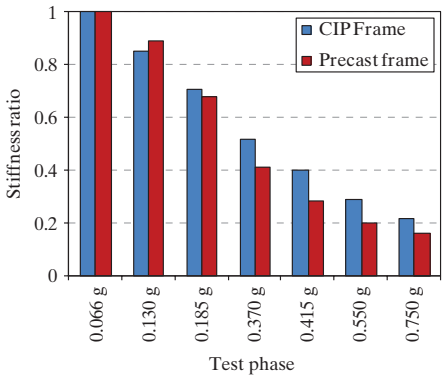

Fig. 7: Stiffness degradation of the two models

hysteresis curves from the earthquake tests, which can reflect the bearing capacity and the change in structural lateral stiffness. This envelop can be obtained through four straight lines joining four key points corresponding to the most distinct stiffness changes. The first point C is due to the first cracks appearing on the model. The second point Y is related to the initial yield stage of the model. Point M represents the maximum load achievement. Finally, point U corresponds to the ultimate load before the model collapse.

Obviously, both the models showed a similar seismic behavior. After the achievement of maximum load, the stiffness degradation was relatively fast for both the models. The figure also indicates that, for the precast frame, the bearing capacity was lower.

Ductility Coefficient

The ductility coefficient is defined by calculating the ratio $\mu = \Delta_u/\Delta_y$ to evaluate the ductility of the two RAC frames. *Table 3* reports the values of key points on the two envelop curves. The ductility coefficient of the CIP frame was calculated and it was

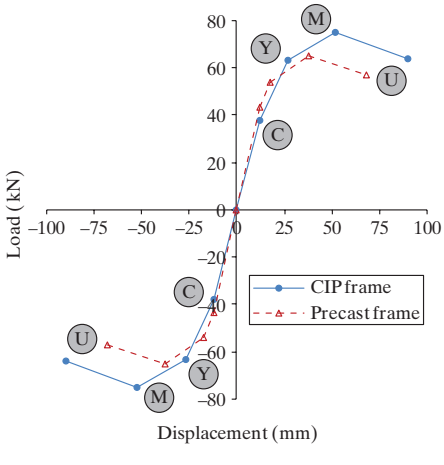

Fig. 8: Envelop curves of the two models

Key points	Parameters	CIP model	Precast model	Variation (%)
C (Cracking)	P_c : kN	37.9	43.4	–14.5
	Δ_c : mm	11.9	11.9	0.0
Y (Yielding)	P_y : kN	63.4	53.9	15.0
	Δ_y : mm	27.0	17.7	34.4
M (Maximum)	P_m : kN	74.8	64.8	13.3
	Δ_m : mm	52.0	37.9	27.1
U (Ultimate)	P_u : kN	63.6	57.1	10.2
	Δ_u : mm	89.5	68.1	23.9

Table 3: Key points of the envelop curves

$\mu_1 = \Delta_{u1}/\Delta_{y1} = 89.50/26.97 = 3.32$ while that of the precast frame was $\mu_2 = \Delta_{u2}/\Delta_{y2} = 68.11/17.68 = 3.85$. The values indicated are for the two models, both showing a good ductile behavior. Though the maximum bearing capacity of the precast model was less than that of the CIP model, the ductility coefficient of the precast model was slightly larger.

Frame Joint Analysis

Seismic Response of Joints

The seismic damage of concrete frame structures occurred mainly at the ends of beams and columns, also in the core areas of joints, and this was observed in numerous earthquake shocks.[29] Because of the complexity of stress in frame joints, its failure will lead to the invalidation or collapse of the structure. Therefore, analysis of the failure process and seismic performance of the frame joints of the two models will probably give an elementary understanding regarding the seismic difference between CIP and precast RAC frame structures.

The lateral force of the i^{th} floor can derived as follows:

$$V_i = \sum_{j=i}^{n} F_j \qquad (2)$$

where V_i is the lateral force of the i^{th} floor and n represents the total number of floors in the structure.

Figure 9 presents the lateral force of the first to fifth floor frame joints during test cases with a PGA of 0.066 *g* (frequently occurring earthquakes of intensity 7), 0.370 *g* (occasionally occurring earthquakes of intensity 8), and 0.750 *g* (maximum considered events). It can be observed from *Fig. 9* that the lateral force of both the models demonstrated a decreasing tendency along the floor height direction and the lateral force of the fourth to fifth floors was always very small through-

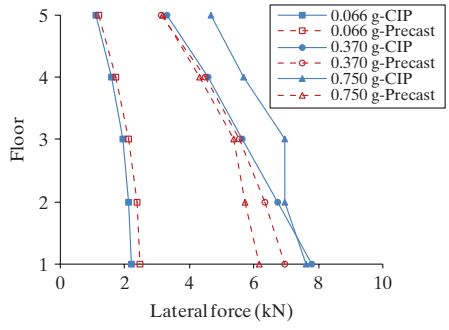

Fig. 9: Lateral force of the two frame joints

out the tests. As for the difference, the lateral force of a precast frame with post-cast joints was greater than in the CIP model in the test case with PGA of 0.066 *g* (frequently occurring earthquakes of intensity 7). On the contrary, the lateral force of precast frame joints was less than that of CIP frame joints in the test cases with PGAs of 0.370 *g* (occasionally occurring earthquakes of intensity 8) and 0.750 *g* (maximum considered events). This demonstrates that the stiffness of the precast frame joints was smaller compared to that of the CIP frame joints at this moment. Based on the observations during the tests, the main reason for a faster lateral stiffness degradation of the precast frame may have been the rapid failure of post-cast joints in earthquake actions of high-level intensity.

Lateral Stiffness Degradation of Joints

Just like the analysis of the stiffness degradation for the two models, Eq. (1) can also be adopted to calculate the stiffness degradation of the frame joints.

$$K_i^j = \frac{\left|+F_i^j\right| + \left|-F_i^j\right|}{\left|+X_i^j\right| + \left|-X_i^j\right|} \qquad (3)$$

where K_i^j is the secant stiffness of the i^{th} test case for the j^{th} floor joint; F_i^j is the lateral force of the pick point in the i^{th} test case for the j^{th} floor joint; and X_i^j is the displacement of the pick

point in the i^{th} test case for the j^{th} floor joint.

Figure 10 compares the stiffness degradation of the first and second floor joints for the two models. It can be observed that the stiffness degradation trend of joints on the first and second floors of the two structures was relative with respect to each other. In the first half of the tests, the frame joint stiffness was basically the same for the two models with almost overlapping degradation curves; however, during the later stages of the tests, the frame joint stiffness of the precast frame was less than that of the CIP frame joint, with a comparatively large decay rate.

Calculation Analysis

Based on the column shear, the maximum joint shear $V_{j,u}$ can be determined[30] as follows:

$$V_{j,u} = \frac{M_{peak}}{0.9d} - V_{c,peak} \quad (4)$$

The calculating formula for the nominal joint shear capacity for frames is defined by ACI 318-08.[26]

$$V_{j,n} = 0.083\gamma\sqrt{f_c'}\,b_j h_c \quad (5)$$

where M_{peak} is the maximum value of the bending moment on X direction of the joint; d is the height of the beam cross section; $V_{c,peak}$ is the maximum column shear; constant γ depends on the connection classification according to ACI 352R-02, here $\gamma = 12$; b_j is the effective joint width; h_c is the height of the column cross section; and f_c is the specified compressive strength of concrete.

A further comparison is listed in *Table 4* based on the above equations for the first and second floor joints of the two models. It can be concluded from the test results that the maximum shear capacity of a frame joint on the CIP frame was larger than that on a precast frame. Adopting the shear capacity formula in the ACI 318-08 for the concrete structure directly is safe for the joint of the CIP frame, while it is somewhat improper for the calculation of the post-cast joint of the precast RAC frame. Introducing some necessary parameters such as the interface influence coefficient to calculate the precast RAC post-cast joint is suggested if this kind of structure is applied in practice. However, this needs to be investigated further in the future.

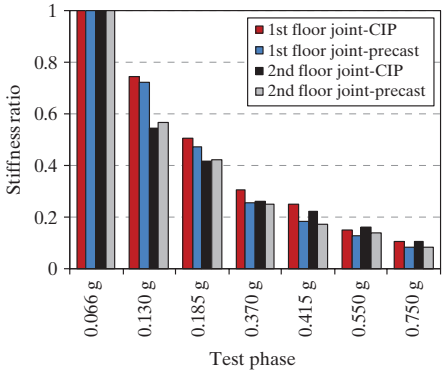

Fig. 10: Stiffness degradation of first and second floor joints

Joint		Test value $V_{j,u}$: kN	ACI 352R-02 $V_{j,n}$: kN	$V_{j,u}/V_{j,n}$
first floor	CIP	44.49	40.14	1.11
	Precast	38.56	40.14	0.96
second floor	CIP	49.57	40.24	1.23
	Precast	42.33	40.24	1.05

Table 4: Comparison of tested and calculated shear capacity of frame joints

Remarks

1. The above analysis reveals that the seismic behavior of a post-cast joint is not inferior to that of the joint of a CIP frame under earthquakes of low intensity; however, it is damaged relatively faster and more seriously with more shear cracks during strong earthquakes, leading to a lower seismic performance. The relatively severe damage level of a post-cast joint is the main reason for the overall lower seismic performance of the precast structure compared to the CIP frame, during an earthquake of high-level intensity.
2. In order to improve the shear capacity and prevent cracks or damages occurring between the interface of the old and new concrete in a post-cast RAC joint, some measurements should be taken to strengthen the shear transfer between the post-cast joint and the precast concrete elements in the joint area. As a result, the progressive connection in a precast system is a new topic if it is to be applied in precast RAC structures.

Conclusions

The construction and test details of the CIP and precast RAC frame model structures have been described in this paper. Comparisons of the seismic behavior as well as a further seismic analysis of the frame joints of the two models have also been presented. The following conclusions have been made:

1. The overall seismic performance of a precast RAC frame is favorable in the elastic and early nonlinear stage, which is almost similar to that of a CIP RAC frame. Although in the later nonlinear stage after the frames had suffered several strong earthquakes, the damage level of a post-cast joint in a precast RAC frame was relatively more serious than that in a CIP RAC frame, with more plastic hinges at the ends of beams and shear cracks in the joint core area, the structural lateral stiffness degradation was a bit faster.
2. In the first half of the tests, the differences in the dynamic seismic response between the two models were quite small; however, in the later part of the shaking table tests, the variation of natural frequency and damping ratio of the precast frame was slightly larger than that of the CIP frame. The damage to a precast RAC frame was somewhat more severe than that to an NAC, during high- intensity earthquake actions. However, the shapes of the lateral deformations of the two frames were basically the same, though the displacement response of the precast frame was greater than that of the CIP frame when the models moved into the nonlinear stage.
3. The comparison of the stiffness degradation and envelop curves showed that the lateral resistances of the two structures were basically the same in the first half of the tests, whereas, after the maximum load achievement, the stiffness of the precast frame decreased faster than that of the CIP frame as seen in the major shear cracks in the models. It was also observed from the envelop curves that, for the precast frame, the bearing capacity was lower; however, calculation of the ductility revealed that both the structures showed a favorable seismic performance.
4. The intensive analysis of the frame joints of the two models showed that the relatively serious damage level of a post-cast joint after a strong earthquake action was the main reason for the inferior seismic behavior of the precast frame compared to the

CIP frame. It was also suggested that some effective measurements should be taken to strengthen the shear transfer between the post-cast joint and the precast concrete elements in the joint area for the precast frame.

Acknowledgements

The authors wish to acknowledge the financial support from the National Natural Science Foundation of China (NSFC) (No: 51325802) and the Shanghai Science and Technique Committee (No. 14231201300).

References

[1] Ding T, Xiao JZ. Estimation of building-related construction and demolition waste in Shanghai. *Waste Manage.* 2014; **34**(11): 2327–2334.

[2] Marinković S, Radonjanin V, Malešev M, Ignjatović I. Comparative environmental assessment of natural and recycled aggregate concrete. Waste Manage. 2010; **30**(11): 2255–2264.

[3] Nixon PJ. Recycled concrete as an aggregate for concrete—a review. *Mater. Struct.* 1978; **11**(65): 371–378.

[4] Hansen TC. Recycled aggregate and recycled aggregate concrete, second state-of-the-art report, developments from 1945–1985. *Mater. Struct.* 1986; **19**(111): 201–246.

[5] Hansen TC. *Recycling of Demolished Concrete and Masonry*. E&FN Spon: London, 1990.

[6] Xiao JZ, Li J, Zhang C. Mechanical properties of recycled aggregate concrete under uniaxial loading. Cement Concrete Res. 2005; **35**(6): 1187–1194.

[7] Xiao JZ, Li L, Tam VWY, Li H. The state of the art regarding the long-term properties of recycled aggregate concrete. *Struct. Concr.* 2014; **15**(1): 3–12.

[8] Poon CS, Chan D. The use of recycled aggregate in concrete in Hong Kong. *Resour. Conserv. Recy.* 2007; **50**(3): 293–305.

[9] Sato R, Maruyama I, Sogabe T, Sogo M. Flexural behavior of reinforced recycled concrete beams. *J. Adv. Concr. Technol*. 2007; **5**(1): 43–61.

[10] Fathifazl G, Razaqpur AG, Isgor OB, Abbas A, Fournier B, Foo S. Shear strength of reinforced recycled concrete beams with stirrups. *Mag. Concrete Res.* 2010; **62**(10): 685–699.

[11] Xiao JZ, Huang X, Shen LM. Seismic behavior of a semi-precast column with recycled aggregate concrete. *Constr. Build. Mater*. 2012; **35**: 988–1001.

[12] Corinaldesi V, Moriconi G. Behavior of beam-column joints made of sustainable concrete under cyclic loading. *J. Mater. Civil Eng.* 2006; **18**(5): 650–658.

[13] Corinaldesi V, Letelier V, Moriconi G. Behavior of beam–column joints made of recycled aggregate concrete under cyclic loading. *Constr. Build. Mater.* 2011; **25**(4): 1877–1882.

[14] Xiao JZ, Sun YD, Falkner H. Seismic performance of frame structures with recycled aggregate concrete. *Eng. Struct*. 2006; **28**(1): 1–8.

[15] Zhang JW, Cao WL, Meng SB, Yu C, Dong HY. Shaking table experimental study of recycled concrete frame–shear wall structures. *Earthq. Eng. Eng. Vib.* 2014; **13**(2): 257–267.

[16] Lu XL. Precast concrete structures in the future. *Struct. Concr.* 2014; **15**(1): 1–2.

[17] Korkmaz HH, Tankut T. Performance of a precast concrete beam-to-beam connection subject to reversed cyclic loading. *Eng. Struct.* 2005; **27**(9): 1392–1407.

[18] Khoo JH, Li B, Yip WK. Tests on precast concrete frames with connections constructed away from column faces. *ACI Struct. J.* 2006; **103**(1): 18–27.

[19] Psycharis IN, Mouzakis HP. Assessment of the seismic design of precast frames with pinned connections from shaking table tests. *B. Earthq. Eng.* 2012; **10**(6): 1795–1817.

[20] Priestley MJN, Sritharan S, James RC, Pampanin S. Preliminary results and conclusions from the PRESSS five-story precast concrete test building. *PCI J.* 1999; **44**(6): 42–67.

[21] Ioani AM, Tripa E. Structural behavior of an innovative all-precast concrete dual system for residential buildings. *PCI J.* 2012; **57**(1): 110–123.

[22] Soutsos MN, Tang KK, Millard SG. Use of recycled demolition aggregate in precast products, phase II: concrete paving blocks. *Constr. Build. Mater.* 2011; **25**(7): 3131–3143.

[23] Soutsos MN, Tang KK, Millard SG. The use of recycled demolition aggregate in precast concrete products – phase III: concrete pavement flags. *Constr. Build. Mater.* 2012; **36**: 674–680.

[24] Xiao JZ, Wang CQ, Li J, Tawana MM Shaking-table model tests on a recycled aggregate concrete frame structure. *ACI Struct. J.* 2012; **109**(6): 777–786.

[25] Sonin AA. A generalization of the Π-theorem and dimensional analysis. *Proc. Natl. Acad. Sci. U S A.* 2004; **101**(23): 8525–8526.

[26] ACI Committee 318. *Building Code Requirements for Structural Concrete (ACI 318-05) and Commentary (ACI 318R-08)*. American Concrete Institute: Farmington Hills, MI, 2008.

[27] Seismology Committee, Recommended Lateral Force Requirements and Commentary (Blue book). Structural Engineers Association of California (SEAOC): California, 1999; 327–421.

[28] Performance-Based Seismic Engineering Ad Hoc Subcommittee. *Revised Interim Guidelines: Performance-based Seismic Engineering for the SEAOC Blue Book*. Structural Engineers Association of California (SEAOC): California, 2003; 128–132.

[29] Meas K, Li B, Imran I. Seismic performance of lightly reinforced concrete exterior beam–column joints. *Adv. Struct. Eng*. 2012; **15**(10): 1765–1780.

[30] Kang T H K, Kim W, Shin M. Cyclic Testing for seismic design guide of beam–column joints with closely spaced headed bars. *J. Earthq. Eng.* 2012; **16**(2): 211–230.